Catalysis Science & Technology

PAPER

View Article Online
View Journal | View Issue

Check for updates

Cite this: *Catal. Sci. Technol.*, 2019, **9**, 1030

Received 25th December 2018,
Accepted 25th January 2019

DOI: 10.1039/c8cy02595a

rsc.li/catalysis

Highly tunable periodic imidazole-based mesoporous polymers as cooperative catalysts for efficient carbon dioxide fixation†

Wei Zhang, ‡[ab] Yu Mei,‡[a] Peng Wu, [a] Hai-Hong Wu *[a] and Ming-Yuan He[a]

The insertion of carbon dioxide (CO_2) into epoxides is a "greener" route for producing cyclic carbonates. Here we report a one-pot synthesis of highly ordered imidazolyl-functionalized mesoporous phenolic resins (IPMPs). We show that the ordering of the IPMP mesostructure depends significantly on the imidazolyl-based precursors. 3-(Imidazole-1-yl)phenol (3-IP) with unoccupied *ortho* and *para* sites was found to be the optimal precursor, yielding a highly ordered cross-linked mesopolymer (3-IPMP) with a high surface area, low density, uniform mesopores and controllable imidazole loading. Control experiments and DFT calculations show that the imidazole doped into the mesoporous organic framework can act synergistically with abundant phenolic hydroxyl groups for co-activation of CO_2 and epoxides, which outperforms the classical periodic mesosilica and polymer-based catalysts. Building on these results, the 3-IPMP mesopolymer was further functionalized with various alkyl halides, forming robust ionic polymers, avoiding the eco-unfriendly addition of KI. In comparison to the porous imidazolium-based poly(ionic liquid), 3-IPMP-EtI, combines the advantages of the imidazole active sites and homogenous KI additive as well as abundant phenolic OH groups in the mesoporous hydrophobic framework, synergistically enhancing its catalytic activity in cycloaddition reactions of CO_2 without the use of any co-catalyst. This novel catalyst is stable and can be reused at least five times without losing activity.

Introduction

Chemical fixation of carbon dioxide (CO_2) has been attracting increased attention because CO_2 is an abundant renewable carbon source.[1] Numerous studies have been reported on the utilization of carbon dioxide (CO_2) as an alternative feedstock for organic synthesis, replacing finite petrochemicals.[2,3] Particularly, the atom-efficient cycloaddition of CO_2 with epoxides is a promising route to produce cyclic carbonates, which are widely used as polar aprotic solvents, electrolytes and intermediates in polycarbonate synthesis.[4,5]

Various homogeneous and heterogeneous catalytic systems were reported for this reaction, including organic compounds,[6] metal–salen complexes,[7–9] metal–organic frameworks,[10–15] covalent organic frameworks,[16–18] and porous organic polymers.[19–21] Only a few catalytic systems are capable of converting CO_2 into cyclic carbonates under mild and even ambient conditions, which typically require a combination of Lewis acidic metal ions (Al, Zn, Co and Fe) and nucleophiles (halide) for the activation and the subsequent ring opening of epoxides.[22] For example, North *et al.* reported bimetallic aluminium–salen complexes in the presence of tetrabutylammonium bromide that gave near-quantitative yields of cyclic carbonates at atmospheric CO_2 pressure and room temperature.[23,24] By comparison, metal-free organocatalysts have been scarcely reported for the CO_2–epoxide coupling reaction under such mild operating conditions, due to their reduced substrate activation potential.[25] Yet most of them are efficient only in the presence of high CO_2 pressure and elevated reaction temperature, thereby restricting their practical applications.[26] Recently, multifunctional organocatalysts have been of great interest as they are able to synergistically activate both CO_2 and epoxides in CO_2 transformation.[26] They mainly comprise ionic liquids, N-heterocyclic carbenes, azaphosphatranes, and phenolic and polyhydroxy compounds.[27] Considering catalyst recovery and product separation, supported functional organocatalysts are preferable.[28] Kleij *et al.* reported a series of polyphenol-derived organic compounds, which acted as efficient one-component bifunctional catalysts in CO_2 cycloaddition at reaction temperatures as low as 45 °C.[29] Furthermore,

---

[a] *Shanghai Key Laboratory of Green Chemistry and Chemical Processes, School of Chemistry and Molecular Engineering, East China Normal University, 3663 North Zhongshan Road, Shanghai, 200062, China. E-mail: hhwu@chem.ecnu.edu.cn; Fax: +86 21 62238510*

[b] *Van 't Hoff Institute for Molecular Sciences, University of Amsterdam, Science Park 904, 1098 XH, Amsterdam, The Netherlands*

† Electronic supplementary information (ESI) available. See DOI: 10.1039/c8cy02595a

‡ These authors contributed equally to this work.

these active moieties were easily immobilized onto polystyrene supports, yielding recyclable heterogeneous catalysts that showed excellent catalytic activities and turnover frequencies comparable to metal-based systems.[25,30] Despite these achievements, however, developing cost-effective and metal-free multifunctional heterogeneous organocatalysts is still essential for the CO_2–epoxide coupling reaction under mild conditions.

Particularly, imidazolium-based ionic liquids are excellent metal-free catalysts owing to their distinctive properties, such as low vapor pressure, good stability and tunable structure.[31–34] Importantly, imidazolium cations show a high affinity to CO_2 *via* dipole–quadruple interactions, which can synergistically catalyze the CO_2–epoxide coupling reaction with nucleophilic halide anions.[35] Typically, imidazole compounds are immobilized on various solid supports such as carbon materials, porous polymers, metal organic frameworks, zeolites, *etc.*[36–39] Specifically, these solid supports bearing hydrogen bond donor groups (*e.g.*, –OH and –NH) can activate epoxides through hydrogen bonding, facilitating the ring opening and subsequent CO_2 insertion.[40,41] Zhang *et al.* showed that chitosan-supported imidazolium ionic liquids can enhance the catalytic performance, which was attributed to the hydrogen bond-assisted epoxide activation.[42] We recently reported imidazolium ionic liquids supported on FDU-type mesopolymers for chemical fixation of CO_2 to give cyclic carbonates in good yields, owing to the combination of the phenolic hydroxyl groups and mesoporous organic framework.[43] For these tailor-made catalysts, however, the active species loading is restricted by the support surface area, and distributing the sites homogenously on the surface is problematic at high loading.[44]

The rational incorporation of imidazole-functional groups into the material skeleton could result in enhanced activity in the CO_2 fixation reaction.[45] Most recently, Wang *et al.* reported a one-step synthesis of imidazole-based porous hyper-crosslinked ionic polymers for the efficient cycloaddition of CO_2 with epoxides.[46,47] Nevertheless, these types of hybrid materials have flexible crosslinked molecular chains, resulting in disordered porous structures. On the other hand, nearly all imidazole-containing polymers with an ordered mesoporous framework typically prepared by a hard-templating method,[48] associated with a harsh etching process.[49] We recently reported a new synthesis method of ordered imidazolyl-functionalized mesoporous polymers, which are comprised of a three-dimensionally rigid framework with a large surface area, low density and high thermal/chemical stability.[50] However, our preliminary tests showed that the ordering of the mesoporous structure significantly decreased with increasing imidazole loading. A facile tunable synthesis of highly ordered mesoporous polymers with high imidazole loading is still a great challenge.

Herein, we report a bottom-up route to a series of highly ordered imidazolyl-functionalized mesoporous polymers (IPMPs) *via* direct co-assembly of imidazole-based precursors and phenolic resol in the presence of a triblock copolymer as a templating agent. Following on our previous work, we opted to systematically study the effect of various imidazolyl-containing precursors on the periodic mesostructures of the IPMP materials. 3-(Imidazole-1-yl)phenol (3-IP), bearing the imidazolyl group in the *meta*-position of the phenol, was the optimal precursor. The resultant 3-IP derived material (3-IPMP) has a highly cross-linked ordered mesoporous network, featuring a large specific surface area, uniform mesoporosity and controllable imidazole loading. In comparison with homogeneous imidazole-base ionic liquids and classical imidazole-containing mesosilica/polymers, 3-IPMP combines the advantages of highly dispersed imidazole species and abundant phenolic hydroxyl groups in the mesoporous hydrophobic framework, resulting in cooperative catalysis and showing superior catalytic activity, selectivity and stability in CO_2 cycloaddition. We also conducted control experiments and DFT calculations, revealing structure–activity relationships in the CO_2–epoxide coupling reaction over the IPMP mesopolymers.

Results and discussion

Catalyst synthesis and characterization of IPMP mesopolymers

We chose three imidazolyl functionalized phenols as precursors: 2-(imidazole-1-yl)phenol (2-IP), 3-(imidazole-1-yl)phenol (3-IP) and 4-(imidazole-1-yl)phenol (4-IP). Fig. 1 briefly illustrates the schematic synthesis of IPMP mesopolymers. First, 3-IP, as an imidazole precursor, interacted with formaldehyde and phenol, and then the obtained imidazole-based oligomers were assembled with the amphiphilic triblock copolymer F127 as a templating agent *via* an evaporation-induced self-assembly method. The subsequent calcination removed the template, producing a highly ordered imidazolyl-functionalized mesoporous polymer (3-IPMP). Similarly, 2-IPMP and 4-IPMP mesopolymers were prepared, starting from 2-IP and 4-IP as imidazole-containing precursors, respectively (see the Experimental section for details in the ESI†).

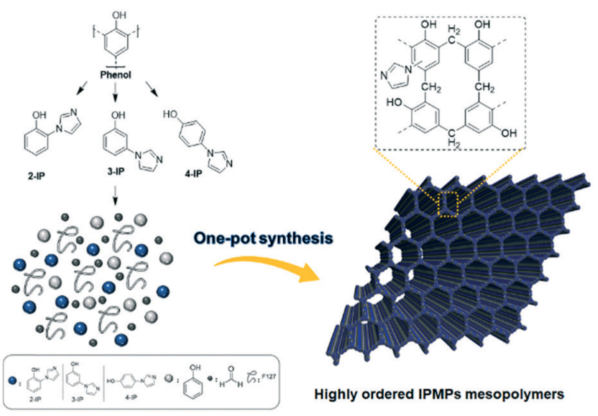

Fig. 1 Illustration of the one-pot synthesis route of highly ordered IPMP mesopolymers.

Small angle X-ray diffraction (XRD) can verify the ordered mesoporous structure of the IPMP samples. As shown in Fig. 2a, the XRD patterns of both 3-IPMP and 4-IPMP exhibit three well-resolved peaks, which are attributed to the (10), (20) and (21) planes of 2D hexagonal *p*6*mm* symmetry.[51] This indicates that 3- and 4-IPMP have a well-ordered mesoporous structure. In addition, the diffraction peaks of 4-IPMP (Fig. 2a, inset) were observed in the lower angle region compared to those of 3-IPMP, which suggests the formation of larger *d*-spacing and unit cell parameters.[52] For 2-IPMP, however, no typical diffraction peaks were detected, implying the long-range disordering of the 2-IP-derived mesopolymer.[53] The nitrogen sorption analysis supports the XRD results. Fig. 2b shows the N_2 adsorption–desorption isotherms of the IPMP materials. All these samples presented type-IV curves with an H1-type hysteresis loop characteristic of mesoporous materials.[54] Specifically, 3- and 4-IP based IPMPs gave a sharp capillary condensation step at relative pressure (P/P_0) from 0.6 to 0.8, indicating a uniform mesoporosity.[55] However, when 2-IP was used as an imidazole precursor, the capillary condensation step became broad and shifted to high relative pressure (P/P_0 = 0.9–1.0), which suggested the formation of numerous interparticle textural pores in 2-IPMP.[56] This trend matched well with the results of the BJH adsorption pore size distribution. As shown in Fig. 2c, both 3-IPMP and 4-IPMP showed a sharp peak evidencing the narrow pore size distribution. The latter has a mean pore size centered at 11.3 nm, which is larger than that of 3-IPMP (8.5 nm). In contrast, 2-IPMP has a broad pore size distribution. The corresponding textural parameters are summarized in Table S1.† Among the three IPMP samples, 3-IPMP has the largest BET surface area (446 m^2 g^{-1}) and pore volume (0.67 cm^3 g^{-1}), which are higher than those of 4-IPMP (440 m^2 g^{-1}, 0.59 cm^3 g^{-1}) and 2-IPMP (253 m^2 g^{-1}, 0.56 cm^3 g^{-1}). Fig. 2d and e show the representative transmission electron microscopy (TEM) images of 3-IPMP viewed from the 10 and 11 directions, which further confirmed the highly ordered 2D hexagonal *p*6*mm* mesoporous structure.[35] For comparison, the TEM images of 2-IPMP and 4-IPMP are given in Fig. S1.† Evidently, 2-IPMP has a typical mesostructure with disordered characteristics, while a structural distortion can be seen in 4-IPMP.

These results indicated the key role of imidazolyl-based precursors in the formation of ordered mesopolymers. As shown in Fig. 2f, the structural difference between these precursors is the imidazolyl substituent located in the *ortho*, *meta* and *para* positions of the phenol ring (with respect to the hydroxyl group), respectively. It's well known that formaldehyde can react with unoccupied *ortho* and *para* sites of the phenol during a base-catalyzed phenolic resin synthesis.[57,58] This explains why *ortho*-substituted and *para*-substituted isomers (2-IP and 4-IP) lower the ordering of the IPMP mesostructures. Besides the substituent effect, 2-IP possesses a disordered mesostructure because of the steric hindrance in *ortho* sites. Therefore, 3-IP has free *ortho*/*para* active sites in phenol, which is more reactive towards formaldehyde than 4-IP in the condensation reaction. This led to a long-range ordering of the 3-IPMP mesopolymer.

The successful incorporation of imidazolyl groups in the IPMP mesopolymers was confirmed by various techniques. The FT-IR spectra of 3-IPMP show new characteristic

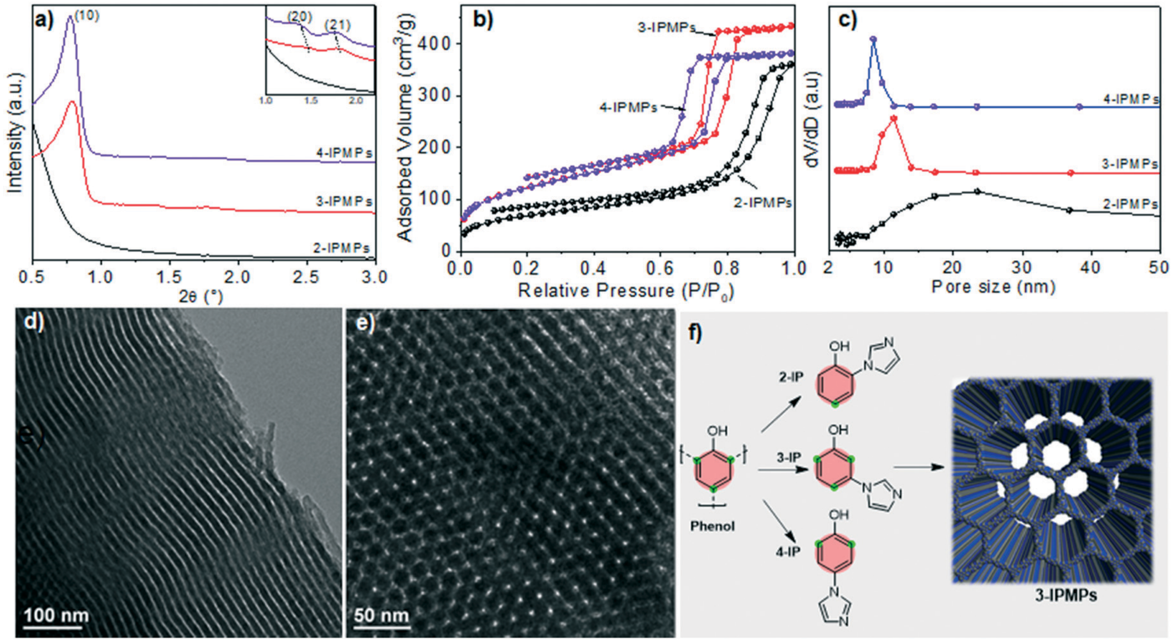

Fig. 2 (a) Small-angle X-ray diffraction patterns, (b) nitrogen adsorption–desorption isotherms and (c) BJH pore size distribution curves of IPMP materials prepared from different imidazole precursors. (d and e) The representative TEM images of the 3-IPMP mesopolymer taken along the 10 direction and 11 direction. (f) Proposed mechanism for the condensation of *ortho*, *meta* and *para*- substituted phenol (2-IP, 3-IP and 4-IP) with formaldehyde.

absorption bands at 3126 cm^{-1}, 1153 cm^{-1}, 1078 cm^{-1} and 827 cm^{-1} (Fig. 3a), in comparison with that of the pure mesoporous polymer (MP) without the addition of 3-IP. These bands can be attributed to the vibrations of the imidazole ring.[59,60] This was also verified by the solid state ^{13}C MAS NMR spectra (Fig. S2†). We then carried out X-ray photoelectron spectroscopy (XPS) measurements to identify the chemical species on 3-IPMP. The N1s peak was deconvoluted into two peaks centered at 400.5 eV and 398.5 eV, assigned to pyrrolic-N and pyridinic-N in the imidazole ring.[42,61] Moreover, we prepared a series of 3-IPMPs with varying imidazole loading, and found that the nitrogen content of the 3-IPMP samples determined by CHN element analysis matched well with the theoretical values (Table S2†). Thermogravimetric analysis (TGA) in an N_2 flow revealed the high thermal stability of 3-IPMP with the starting decomposition temperature above 400 °C (Fig. S3†). Based on these results, we conclude that imidazole functionalities are completely integrated into the mesoporous polymer framework of the IPMPs.

Catalytic testing

These IPMP mesopolymers were used as heterogeneous catalysts in the cycloaddition of CO_2 with epoxides. Generally, imidazole-containing catalyst systems require a nucleophile (*e.g.*, halide ions), which plays a vital role in the ring-opening of epoxides.[62] Potassium iodide (KI) is a cheap, nontoxic and abundant metal salt. Unlike tetrabutylammonium iodide (TBAI), KI is seldom used as a co-catalyst due to the strong interaction between K^+ and I^-.[63] Han *et al.* reported that KI can catalyze this reaction in the presence of a hydroxyl substance.[64] We therefore reasoned that our IPMP mesopolymers would be simple and cost-effective catalysts for the CO_2–epoxide coupling reaction in the presence of KI.

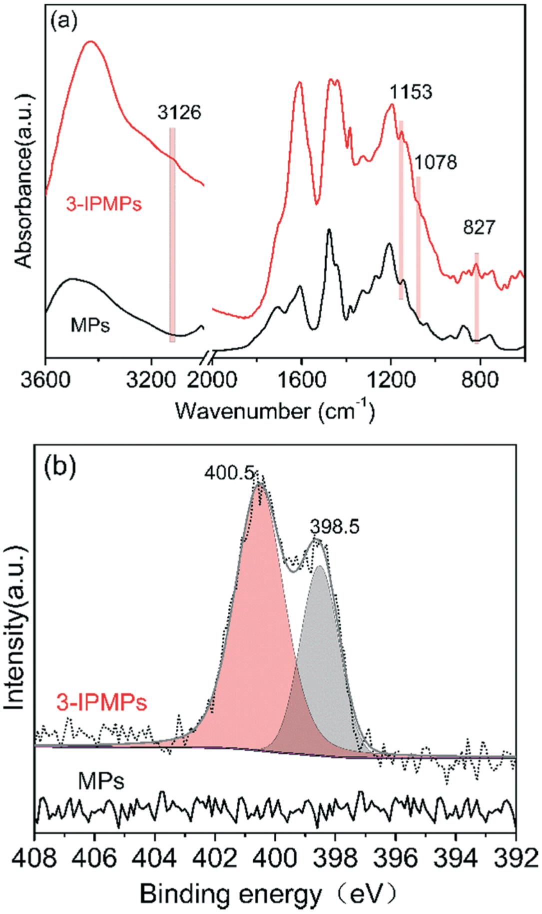

Fig. 3 FT-IR spectra (a) and high-resolution N 1s spectra (b) of 3-IPMP and the pure mesoporous polymer (MP) without the addition of 3-IP.

Initially, we chose the cycloaddition of CO_2 with propylene oxide as a model reaction (eqn (1)) with KI as a co-catalyst under 1 MPa CO_2 pressure at 90 °C for 1 h. The results are summarized in Table 1. Control experiments confirmed that no product was detected in the absence of IPMPs (entry 1), suggesting that KI scarcely catalyzed the reaction. The IMMPs themselves are active but gave a low yield (12%, entry 2). Remarkably, all the IPMP catalysts showed good activity and high turnover frequencies (TOF) in combination with the KI additive (entries 3–5). This indicates that the IPMP mesopolymers act synergistically with KI to promote the CO_2 cycloaddition reaction. Among them, 3-IPMP gave the highest yield of 77% of propylene carbonate. We further studied imidazole catalysts supported on three classical supports: polystyrene (PS), periodic mesosilica SBA-15 and highly ordered mesoporous phenolic resins (FDU-15), aiming to understand the high performance of the IPMP catalysts. For comparison, we prepared these supported imidazole catalysts by a post-modification method with identical imidazole loading, and the textual parameters are summarized in Table S1.† To our delight, these supported imidazole catalysts gave less propylene carbonate compared with 3-IPMP (Table 1, entries 6–8). The PS polymer is composed of a connected benzene ring skeleton similar to our IPMPs, albeit the absence of phenolic hydroxyl groups, may explain the lower activity. Note that both SBA-15 and FDU-15 have an ordered 2D hexagonal *p6mm* mesostructure, and the specific surface area of the imidazole/SBA-15 catalyst is 623 m^2 g^{-1}, much higher than that of imidazole/FDU-15 (391 m^2 g^{-1}). However, the latter gave a much higher yield (51%) and TOF value (103 h^{-1}), confirming further the importance of the phenolic hydroxyl groups in the mesoporous hydrophobic framework. In addition, direct doping of imidazole into the mesoporous polymer (IPMP) can avoid the blockage of pores during the synthesis. Indeed, 3- IPMP gave a larger mesopore size of 8.5 nm, compared to 6.7 nm for the FDU-15 supported imidazole. Owing to the combination of a high surface area, well-dispersed imidazole species and abundant phenolic hydroxyl groups in the mesoporous hydrophobic framework, the highly ordered 3-IPMP showed an enhanced catalytic activity in cycloaddition of CO_2. We also investigated the influence of the reaction parameters including the reaction temperature, CO_2 pressure, amount of catalyst and reaction time. The results are summarized in Table S3.† 3-IPMP gave a near-quantitative yield of propylene carbonate under optimal conditions of 1 MPa, 90 °C, and 0.5 mol% catalyst amount for 3 h.

Table 1 Cycloaddition of CO_2 to propylene oxide over various catalysts[a]

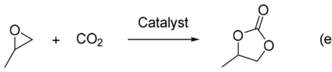

(eq 1)

Entry	Catalyst	Yield[b] (%)	Selectivity[b] (%)	TOF[c] (h^{-1})
1[d]	KI	Trace	—	—
2[e]	3-IPMP	12	99	24
3	2-IPMP	40	99	81
4	4-IPMP	64	99	129
5	3-IPMP	77	99	156
6	Imidazole/PS	18	99	36
7	Imidazole/SBA-15	27	99	55
8	Imidazole/FDU-15	51	99	103

[a] Reaction conditions: propylene oxide 30 mmol, catalyst 0.5 mol% (imidazole loading was determined by element analysis), KI 2 mol% (0.6 mmol, 100 mg), 1 MPa CO_2, 90 °C, 1 h. [b] Determined by GC using biphenyl as an internal standard. [c] Turnover frequency (TOF) for propylene carbonate formation calculated as moles of propylene oxide per mole of imidazole loading per hour. [d] No catalyst (only KI). [e] No KI co-catalyst was added.

To gain insight into the structure–activity relationships in CO_2 cycloaddition over IPMPs, we then performed density functional theory (DFT) calculations. Although 3-IPMP and 4-IPMP have a similar mesostructure and comparable textual parameters (see Table S1†), 3-IPMP showed superior catalytic performance (Table 1, entries 4 *vs.* 5). We reasoned that the reaction is substituent-sensitive, and the imidazole located in the *meta* site (3-IP) is more favorable than that in the *para* site (2-IP). To simplify this, we studied the interaction among propylene oxide, CO_2 and 2-/3-IP using the CP2K software package *via* the combined Gaussian and plane-wave (GPW) method.[65] As shown in Fig. 4, geometry optimization showed that both 3-IP and 4-IP can form hydrogen bonds with propylene oxide *via* the phenolic hydroxyl groups. As expected, 3-IP forms a shorter H bond (2.719 Å) with propylene oxide in comparison with 4-IP (2.884 Å). This indicates that the H bond donating capacity of 3-IP is superior to that of 4-IP. Moreover, the computations showed that the imidazolyl group of the IP can polarize and activate CO_2. For CO_2–3-IP, the bond angle of linear CO_2 was bent to 176.1° and the CO_2 coordinates to the imidazole N atom with a much shorter C⋯N distance of 2.814 Å, in comparison with CO_2–3-IP (176.9°, 3.884 Å). Shortening the distances with reactants (CO_2 and epoxide) can boost the catalytic efficiency. Thus, the simulations show us why 3-IP is more reactive than 4-IP; the former acts as a 'catalytic shuttle', especially under the real dynamic conditions.

Adding KI as a co-catalyst is a facile approach for accelerating the CO_2 cycloaddition reaction.[66] However, the extra potassium salt makes this process unsustainable. To address this problem, the IPMP mesopolymers were further functionalized with various alkyl halides, yielding recyclable ionic polymers with halogen counteranions (*i.e.*, IPMP-derived ionic liquids). We reasoned that the abundant imidazolium-halide ion pairs in the ionic polymers synergistically enhanced their activities in the cycloaddition of CO_2 to epoxides without any additives.[67] Scheme 1 briefly outlines the synthesis of IPMP-derived ionic liquids *via* a simple alkylation of IPMPs with bromoethane (EtBr); the resulting samples are denoted as 2-IPMP-EtBr, 3-IPMP-EtBr and 4-IPMP-EtBr, respectively (see the ESI† for details).

As shown in Fig. 5, all the IPMP-EtBr ionic polymers bearing imidazolium cations and nucleophilic Br anions proved to be highly active and outperformed the control combination of {IPMP + KI}. More importantly, these IPMP-derived ionic polymers are stable and easily separated by simple filtration. They can be reused at least five times without losing

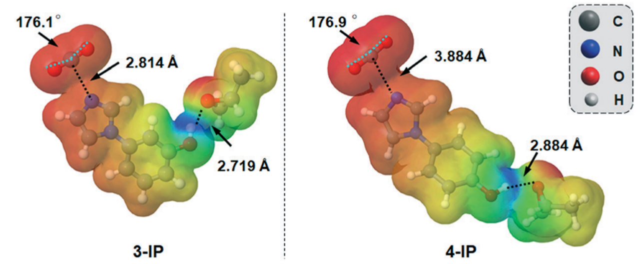

Fig. 4 The optimized geometries: 3-IP interacts with CO_2 and propylene oxide; 4-IP interacts with CO_2 and propylene oxide.

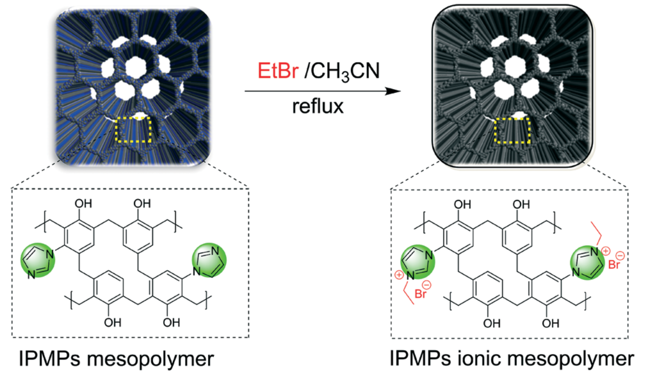

Scheme 1 Schematic illustration of the synthesis of IPMP-derived ionic liquids *via* a simple alkylation of IPMPs with bromoethane (EtBr).

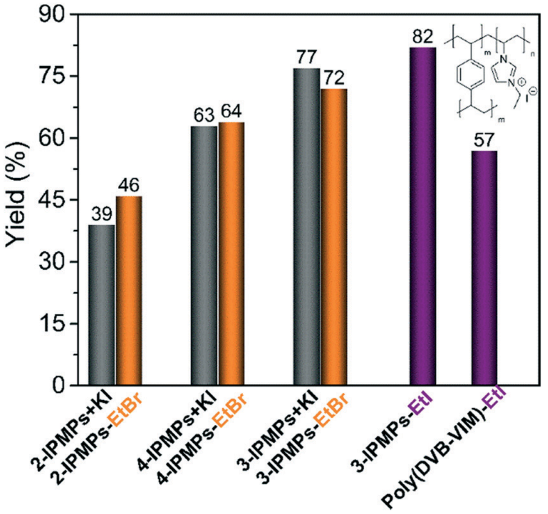

Fig. 5 Comparisons of propylene carbonate yields over the {IPMPs + KI} combination, IPMP-EtBr, 3-IPMP-EtI and poly(DVB–VIM)-EtI. Reaction conditions: propylene oxide 30 mmol, catalyst 0.5 mol% (0.5 mol% imidazole loading relative to the substrate, which was determined by element analysis), 1 MPa CO_2, 90 °C, 3 h. Note: {IPMP + KI} (0.5 mol% each).

activity in the co-catalyst free cycloaddition reaction (see recycling experiments below). The catalytic reactivity in this series was ranked 3-IPMP-EtBr > 4-IPMP-EtBr > 2-IPMP-EtBr, further supporting the simulation results. Additionally, the halide counteranions play a vital role in our reaction. To test this, we prepared 3-IPMP-EtI *via* alkylation of 3-IPMP with iodoethane (EtI) instead of EtBr. 3-IPMP-EtI exhibited the best catalytic activity among all the catalysts tested in this study, giving a higher yield of 82% than 3-IPMP-EtBr (72%). This is probably due to the superior nucleophilicity and leaving ability of I^- to Br^-.[68]

For comparison, we prepared an imidazolium-based poly(ionic liquid) with an identical imidazole content *via* the precipitation–polymerization method using vinylimidazole (VIM) as a monomer and divinylbenzene (DVB) as a cross-linking agent (see the ESI† for details).[69] The resulting ionic polymer was denoted as poly(DVB–VIM)-EtI, and the corresponding porosity analysis is shown in Table S1.† The specific BET surface area of poly(DVB–VIM)-EtI was as high as 600 m^2 g^{-1}, much higher than that of 3-IPMP-EtI (425 m^2 g^{-1}). However, in spite of the high BET surface area, poly(DVB–VIM)-EtI gave a much lower yield (57%) than 3-IPMP-EtI (82%). The highly ordered 3-IPMP-EtI mesopolymer is one of most efficient catalysts for CO_2–epoxide coupling into cyclic carbonates under similar conditions, compared to other previously reported analogous catalysts.[26] Wang *et al.* reported a novel imidazolium- and triazine-based porous ionic polymer (IT-POP-1) for catalytic conversion of CO_2 into propylene carbonate at 1 MPa,[67] which is comparable to our 3-IPMP-EtI. But the reported temperature of 120 °C for the reaction was much higher than that of 3-IPMP-EtI (90 °C). These results confirmed that 3-IPMP-EtI combines the advantages of the imidazole active sites and homogenous KI additive as well as abundant phenolic OH groups in the mesoporous hydrophobic framework, showing an enhanced catalytic performance in the cycloaddition reaction of CO_2 without the use of any co-catalyst.

We also examined the effect of imidazole loading on the catalytic performance by varying the 3-IP precursor concentration for a series of 3-IPMP mesopolymers. These samples are denoted as 3-IPMP-*x*, where *x* represents the molar ratio (mol%) of 3-IP/ (3-IP + phenol) in the synthesis (*x* = 5%, 10%, 20% and 40%). Fig. 6 shows the representative TEM images of these 3-IPMP-*x* samples viewed from the [10] direction. All the samples showed stripe-like and hexagonally arranged pore channels in large domains and a decrease in the ordering of the 2D mesostructure with increasing imidazole loading. Examining the mesoporosity of 3-IPMP-*x* by N_2 sorption analysis supported this observation (Fig. S4†), and the corresponding textual parameters are summarized in Table S4.† These 3-IPMP-*x* samples were then reacted with iodoethane (EtI) to give the corresponding ionic polymers (denoted as 3-IPMP-EtI-*x*). Fig. 7 shows the TON and yield profiles of these 3-IPMP-EtI catalysts. The 3-IPMP-EtI-0 catalyst without an imidazole dopant scarcely catalyzed the reaction. When the imidazole was incorporated into the mesopolymer, the resultant 3-IPMP-EtI samples showed excellent activity. The yield of propylene carbonate increased from 63% to 82% with an increase in the imidazole loading (from 5% to 20%), indicating that imidazolium ions serves as active sites in CO_2 cycloaddition. Increasing the imidazole loading further retards the reaction, and IPMP-EtI-40 gave a much lower yield of 51%. We then calculated the TON values to evaluate these catalysts. The highest TON of 504 was achieved for 3-IPMP-EtI-5. This is probably because of the fact that more imidazole resulted in a distortion of the mesostructure, lowering the

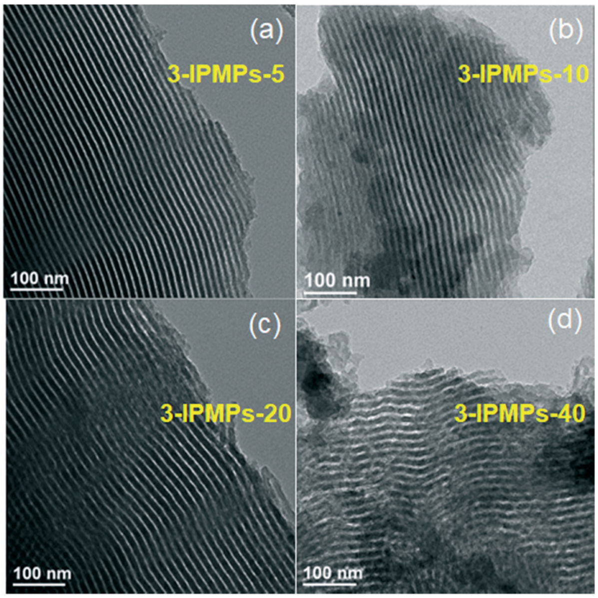

Fig. 6 High-resolution TEM images taken along the [10] direction of 3-IPMP-5 (a), 3-IPMP-10 (b), 3-IPMP-20 (c) and 3-IPMP-40 (d).

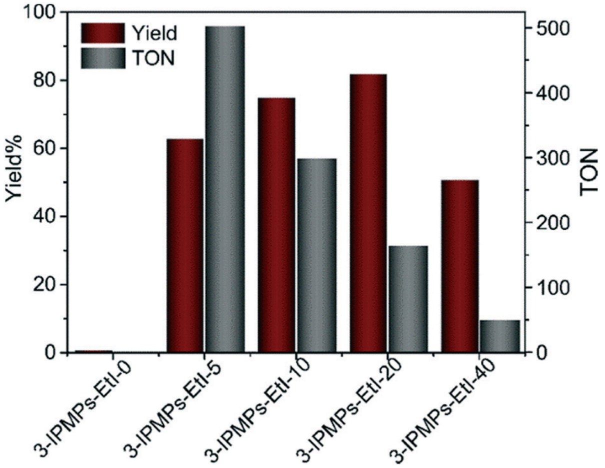

Fig. 7 The relationship between the yield, TON for propylene carbonate formation and imidazole loading of 3-IPMP-EtI catalysts. Reaction conditions: propylene oxide 30 mmol, catalyst 0.5 mol%, 1 MPa CO_2, 90 °C, 3 h.

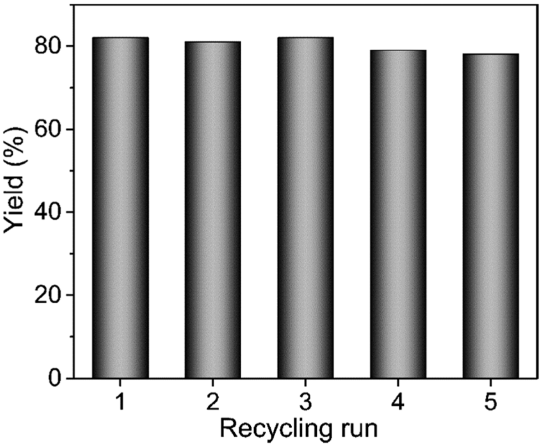

Fig. 8 Recycling of 3-IPMP-EtI in the cycloaddition of CO_2 with propylene oxide. Reaction conditions: propylene oxide 30 mmol, catalyst 0.5 mol%, 1 MPa CO_2, 90 °C, 3 h.

specific surface area of the mesopolymer, thereby leading to inaccessible active sites.

Additionally, the catalytic scope of the 3-IPMP-EtI-20 catalyst for CO_2 cycloaddition with various epoxides was further examined at 90 °C for 5 h under 1 MPa CO_2 (Table 2). All the terminal epoxides bearing electron-withdrawing and electron-donating substituents gave good conversion and selectivity (entries 1–4). The reaction with cyclohexene oxide gave a low conversion (entry 5), confirming the steric hindrance effect.[70]

More importantly, 3-IPMP-EtI-20 is stable. As shown in Fig. 8, the 3-IPMP-EtI-20 catalyst can be separated by simple filtration and reused at least five times without a significant loss of activity. Additionally, the mesostructure and imidazole content of the spent catalyst were well preserved after recycling, as evidenced by XRD (Fig. S5†) and element analysis. Notably, there is a slight decrease in the propylene carbonate yield at the fifth run, due to the leaching of nucleophilic I^- *via* a reverse Menschutkin reaction.[71] This agrees well with the decrease in iodide loading of the recovered catalyst in comparison with the fresh 3-IPMP-EtI (from 16.3% to 11.1% I, determined by ICP-MS analysis). From these results, the highly ordered 3-IPMP mesopolymer is one of most efficient catalysts for CO_2–epoxide coupling into cyclic carbonates under mild conditions.

Table 2 Cycloaddition of CO_2 with various epoxides catalyzed by 3-IPMP-EtI[a]

Entry	Epoxide	Product	Yield[b] (%)	Selectivity[b] (%)
1		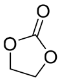	93	99
2		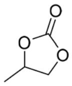	91	99
3	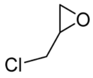	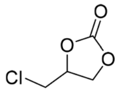	90	99
4	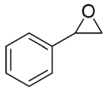	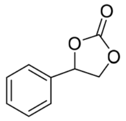	88	99
5[c]	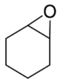	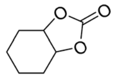	71	99 (*cis*)

[a] Reaction conditions: propylene oxide 30 mmol, 3-IPMP-EtI 0.5 mol% (150 mg), 1 MPa CO_2, 90 °C, 5 h. [b] Determined by GC using biphenyl as an internal standard. [c] 2 MPa, 24 h, product *cis*-cyclohexane carbonate.

Conclusions

We have developed a facile bottom-up strategy for the synthesis of a series of highly ordered imidazolyl-functionalized mesoporous phenolic resins (IPMPs) *via* controllable incorporation of the imidazole moiety into the mesopolymer frameworks. Owing to the free *ortho*/*para* active sites of the phenol ring, 3-(imidazole-1-yl)phenol is the optimal imidazole precursor, forming a well-ordered 2D hexagonal mesopolymer (3-IPMP) with a large specific surface area and uniform pore sizes as well as a mesoporous hydrophobic framework. Given these fantastic properties, 3-IPMP exhibited high catalytic performance for the cycloaddition of CO_2 with epoxides to cyclic carbonates in the presence of a KI co-catalyst. Control experiments and computations showed that the excellent catalytic performance of 3-IPMP arises from the cooperative action of combining abundant imidazolyl and phenolic hydroxyl groups in the hydrophobic mesochannels, activating CO_2 and epoxides in the cycloaddition reaction. Inspired by these findings, we designed a series of novel 3-IPMP derived ionic polymers, in which the imidazolium–halide ion pairs synergistically enhanced their activities in the cycloaddition of CO_2 to epoxides without any additives. The synthesized

3-IPMP-EtI showed high efficiency as a robust catalyst, and can be reused at least five times without losing activity. The simple metal-free solids reported here can offer cooperative catalysis for highly efficient conversion of CO_2 to value-added chemicals under mild conditions, providing fundamental insights for developing cost-effective, metal-free heterogonous organocatalysts for practical implementation of CO_2 transformation.

Conflicts of interest

There are no conflicts to declare.

Acknowledgements

This work is supported by the National Natural Science Foundation of China (21573073), the National Key Research and Development Program of China (2017YFA0403102) and the Shanghai Leading Academic Discipline Project (B409).

References

1 M. He, Y. Sun and B. Han, *Angew. Chem., Int. Ed.*, 2013, **52**, 9620.
2 M. Tamura, M. Honda, Y. Nakagawa and K. Tomishige, *J. Chem. Technol. Biotechnol.*, 2014, **89**, 19.
3 Z.-Z. Yang, L.-N. He, J. Gao, A.-H. Liu and B. Yu, *Energy Environ. Sci.*, 2012, **5**, 6602.
4 X.-B. Lu and D. J. Darensbourg, *Chem. Soc. Rev.*, 2012, **41**, 1462.
5 B. Schaffner, F. Schaffner, S. P. Verevkin and A. Borner, *Chem. Rev.*, 2010, **110**, 4554.
6 S. Zhang, J. Sun, X. Zhang, J. Xin, Q. Miao and J. Wang, *Chem. Soc. Rev.*, 2014, **43**, 7838.
7 T. Zhao, Y. Ren, J. Yang, L. Wang, W. Jiang, A. Elzatahry, A. Alghamdi, Y. Deng, D. Zhao and W. Luo, *J. Mater. Chem. A*, 2016, **4**, 16446.
8 Z. Taşcı and M. Ulusoy, *J. Organomet. Chem.*, 2012, **713**, 104.
9 J. Chun, S. Kang, N. Kang, S. M. Lee, H. J. Kim and S. U. Son, *J. Mater. Chem. A*, 2013, **1**, 5517.
10 L. Tang, S. Zhang, Q. Wu, X. Wang, H. Wu and Z. Jiang, *J. Mater. Chem. A*, 2018, **6**, 2964.
11 J. Liang, Y.-Q. Xie, X.-S. Wang, Q. Wang, T.-T. Liu, Y.-B. Huang and R. Cao, *Chem. Commun.*, 2018, **54**, 342.
12 X.-Y. Li, L.-N. Ma, Y. Liu, L. Hou, Y.-Y. Wang and Z. Zhu, *ACS Appl. Mater. Interfaces*, 2018, **10**, 10965.
13 M. Ding and H.-L. Jiang, *ACS Catal.*, 2018, **8**, 3194.
14 M. Ding, S. Chen, X.-Q. Liu, L.-B. Sun, J. Lu and H.-L. Jiang, *ChemSusChem*, 2017, **10**, 1898.
15 M. Taherimehr, B. Van de Voorde, H. Wee Lik, A. Martens Johan, E. De Vos Dirk and P. Pescarmona Paolo, *ChemSusChem*, 2016, **10**, 1283.
16 Y. Zhi, P. Shao, X. Feng, H. Xia, Y. Zhang, Z. Shi, Y. Mu and X. Liu, *J. Mater. Chem. A*, 2018, **6**, 374.
17 W. Yu, S. Gu, Y. Fu, S. Xiong, C. Pan, Y. Liu and G. Yu, *J. Catal.*, 2018, **362**, 1.
18 O. Buyukcakir, S. H. Je, S. N. Talapaneni, D. Kim and A. Coskun, *ACS Appl. Mater. Interfaces*, 2017, **9**, 7209.
19 Y. Xu, L. Lin, C.-T. He, J. Qin, Z. Li, S. Wang, M. Xiao and Y. Meng, *Polym. Chem.*, 2017, **8**, 3632.
20 Q. Wu, K. Huang, F. Liu, P. Zhang and L. Jiang, *Ind. Eng. Chem. Res.*, 2017, **56**, 15008.
21 Y. Du, H. Yang, S. Wan, Y. Jin and W. Zhang, *J. Mater. Chem. A*, 2017, **5**, 9163.
22 C. Martín, G. Fiorani and A. W. Kleij, *ACS Catal.*, 2015, **5**, 1353.
23 W. Clegg, R. W. Harrington, M. North and R. Pasquale, *Chem. – Eur. J.*, 2010, **16**, 6828.
24 M. North and P. Villuendas, *ChemCatChem*, 2012, **4**, 789.
25 C. J. Whiteoak, A. H. Henseler, C. Ayats, A. W. Kleij and M. A. Pericàs, *Green Chem.*, 2014, **16**, 1552.
26 Q.-W. Song, Z.-H. Zhou and L.-N. He, *Green Chem.*, 2017, **19**, 3707.
27 G. Fiorani, W. Guo and A. W. Kleij, *Green Chem.*, 2015, **17**, 1375.
28 O. Martinez-Ferrate, G. Chacon, F. Bernardi, T. Grehl, P. Bruner and J. Dupont, *Catal. Sci. Technol.*, 2018, **8**, 3081.
29 S. Sopeña, G. Fiorani, C. Martín and A. W. Kleij, *ChemSusChem*, 2015, **8**, 3248.
30 L. Martínez-Rodríguez, J. Otalora Garmilla and A. W. Kleij, *ChemSusChem*, 2016, **9**, 749.
31 C. Yue, D. Su, X. Zhang, W. Wu and L. Xiao, *Catal. Lett.*, 2014, **144**, 1313.
32 J. Sun, S. Zhang, W. Cheng and J. Ren, *Tetrahedron Lett.*, 2008, **49**, 3588.
33 L. Wang, X. Jin, P. Li, J. Zhang, H. He and S. Zhang, *Ind. Eng. Chem. Res.*, 2014, **53**, 8426.
34 M. H. Anthofer, M. E. Wilhelm, M. Cokoja, I. I. E. Markovits, A. Pothig, J. Mink, W. A. Herrmann and F. E. Kuhn, *Catal. Sci. Technol.*, 2014, **4**, 1749.
35 T.-T. Liu, R. Xu, J.-D. Yi, J. Liang, X.-S. Wang, P.-C. Shi, Y.-B. Huang and R. Cao, *ChemCatChem*, 2018, **10**, 2036.
36 J. Liang, R.-P. Chen, X.-Y. Wang, T.-T. Liu, X.-S. Wang, Y.-B. Huang and R. Cao, *Chem. Sci.*, 2017, **8**, 1570.
37 W. Cheng, X. Chen, J. Sun, J. Wang and S. Zhang, *Catal. Today*, 2013, **200**, 117.
38 C. Calabrese, F. Liotta Leonarda, E. Carbonell, F. Giacalone, M. Gruttadauria and C. Aprile, *ChemSusChem*, 2016, **10**, 1202.
39 G. Sneddon, A. Greenaway and H. H. P. Yiu, *Adv. Energy Mater.*, 2014, **4**, 1301873.
40 J. Steinbauer and T. Werner, *ChemSusChem*, 2017, **10**, 3025.
41 T. Wang, X. Song, Q. Luo, X. Yang, S. Chong, J. Zhang and M. Ji, *Microporous Mesoporous Mater.*, 2018, **267**, 84.
42 J. Sun, J. Wang, W. Cheng, J. Zhang, X. Li, S. Zhang and Y. She, *Green Chem.*, 2012, **14**, 654.
43 W. Zhang, Q. Wang, H. Wu, P. Wu and M. He, *Green Chem.*, 2014, **16**, 4767.
44 W. Zhang, G. Innocenti, P. Oulego, V. Gitis, H.-H. Wu, B. Ensing, F. Cavani, G. Rothenberg and N. R. Shiju, *ACS Catal.*, 2018, **8**, 2365.

45 Y. Xie, J. Liang, Y. Fu, M. Huang, X. Xu, H. Wang, S. Tu and J. Li, *J. Mater. Chem. A*, 2018, **6**, 6660.

46 J. Li, D. Jia, Z. Guo, Y. Liu, Y. Lyu, Y. Zhou and J. Wang, *Green Chem.*, 2017, **19**, 2675.

47 Z. Guo, Q. Jiang, Y. Shi, J. Li, X. Yang, W. Hou, Y. Zhou and J. Wang, *ACS Catal.*, 2017, **7**, 6770.

48 J. Huang, C.-A. Tao, Q. An, W. Zhang, Y. Wu, X. Li, D. Shen and G. Li, *Chem. Commun.*, 2010, **46**, 967.

49 A. Thomas, *Angew. Chem., Int. Ed.*, 2010, **49**, 8328.

50 W. Zhang, T. Liu, H. Wu, P. Wu and M. He, *Chem. Commun.*, 2015, **51**, 682.

51 Y. Meng, D. Gu, F. Zhang, Y. Shi, H. Yang, Z. Li, C. Yu, B. Tu and D. Zhao, *Angew. Chem.*, 2005, **117**, 7215.

52 R. Xing, N. Liu, Y. Liu, H. Wu, Y. Jiang, L. Chen, M. He and P. Wu, *Adv. Funct. Mater.*, 2007, **17**, 2455.

53 G. P. Mane, S. N. Talapaneni, C. Anand, S. Varghese, H. Iwai, Q. Ji, K. Ariga, T. Mori and A. Vinu, *Adv. Funct. Mater.*, 2012, **22**, 3596.

54 K. Hou, A. Zhang, L. Gu, M. Liu and X. Guo, *J. Colloid Interface Sci.*, 2012, **377**, 18.

55 R. Xing, H. Wu, X. Li, Z. Zhao, Y. Liu, L. Chen and P. Wu, *J. Mater. Chem.*, 2009, **19**, 4004.

56 W. Zhang, G. Innocenti, M. Ferbinteanu, E. V. Ramos Fernandez, A. Sepulveda-Escribano, H.-H. Wu, F. Cavani, G. Rothenberg and R. N. Shiju, *Catal. Sci. Technol.*, 2018, **8**, 3737.

57 M.-F. Grenier-Loustalot, S. Larroque, P. Grenier, J.-P. Leca and D. Bedel, *Polymer*, 1994, **35**, 3046.

58 I. Muylaert, A. Verberckmoes, J. De Decker and P. Van Der Voort, *Adv. Colloid Interface Sci.*, 2012, **175**, 39.

59 L. Han, H.-J. Choi, S.-J. Choi, B. Liu and D.-W. Park, *Green Chem.*, 2011, **13**, 1023.

60 J. Sun, W. Cheng, W. Fan, Y. Wang, Z. Meng and S. Zhang, *Catal. Today*, 2009, **148**, 361.

61 K. Fahsi, S. G. Dutremez, A. Vioux and L. Viau, *J. Mater. Chem. A*, 2013, **1**, 4451.

62 T. Sakakura and K. Kohno, *Chem. Commun.*, 2009, 1312.

63 Z. Xue, X. Zhao, J. Wang and T. Mu, *Chem. – Asian J.*, 2017, **12**, 2271.

64 J. Ma, J. Liu, Z. Zhang and B. Han, *Green Chem.*, 2012, **14**, 2410.

65 W. Zhang, B. Ensing, G. Rothenberg and R. N. Shiju, *Green Chem.*, 2018, **20**, 1866.

66 Y. Chen, R. Luo, Q. Xu, J. Jiang, X. Zhou and H. Ji, *ChemSusChem*, 2017, **10**, 2534.

67 H. Zhong, Y. Su, X. Chen, X. Li and R. Wang, *ChemSusChem*, 2017, **10**, 4855.

68 J. Steinbauer, L. Longwitz, M. Frank, J. Epping, U. Kragl and T. Werner, *Green Chem.*, 2017, **19**, 4435.

69 A. Dani, E. Groppo, C. Barolo, J. G. Vitillo and S. Bordiga, *J. Mater. Chem. A*, 2015, **3**, 8508.

70 J. Langanke, L. Greiner and W. Leitner, *Green Chem.*, 2013, **15**, 1173.

71 T. Jose, S. Cañellas, M. A. Pericàs and A. W. Kleij, *Green Chem.*, 2017, **19**, 5488.